



Missing mass spectra in hadronic events from e^+e^- collisions at $\sqrt{s}=161-172$ GeV and limits on invisible Higgs decays

M. Acciarri, O. Adriani, M. Aguilar-Benitez, S. Ahlen, J. Alcaraz, G. Alemanni, J. Allaby, A. Aloisio, G. Alverson, M G. Alviggi, et al.

► To cite this version:

M. Acciarri, O. Adriani, M. Aguilar-Benitez, S. Ahlen, J. Alcaraz, et al.. Missing mass spectra in hadronic events from e^+e^- collisions at $\sqrt{s}=161-172$ GeV and limits on invisible Higgs decays. Physics Letters B, 1998, 418, pp.389-398. 10.1016/S0370-2693(97)01394-4 . in2p3-00000019

HAL Id: in2p3-00000019

<https://hal.in2p3.fr/in2p3-00000019>

Submitted on 4 Nov 1998

HAL is a multi-disciplinary open access archive for the deposit and dissemination of scientific research documents, whether they are published or not. The documents may come from teaching and research institutions in France or abroad, or from public or private research centers.

L'archive ouverte pluridisciplinaire **HAL**, est destinée au dépôt et à la diffusion de documents scientifiques de niveau recherche, publiés ou non, émanant des établissements d'enseignement et de recherche français ou étrangers, des laboratoires publics ou privés.

**Missing mass spectra in hadronic events
from e^+e^- collisions at $\sqrt{s}=161\text{-}172$ GeV
and limits on invisible Higgs decays**

L3 Collaboration

Abstract

Events characterised by large hadronic energy and transverse momentum are selected from the data collected by the L3 detector at LEP at centre-of-mass energies between 161 and 172 GeV, corresponding to an integrated luminosity of 21 pb^{-1} . The visible mass and the missing mass distributions of the selected events are consistent with those expected from Standard Model processes. This result is combined with that from data taken at the Z resonance to set an upper limit on the production rate and decay into invisible final states of a non-minimal Higgs boson, as a function of the Higgs mass. Assuming the non-minimal Higgs production cross section to be the same as for the Standard Model Higgs boson and the decay branching fraction into invisible final states to be 100%, a Higgs mass lower limit of 69.6 GeV is derived at 95% confidence level.

Submitted to *Phys. Lett. B*

1 Introduction

This paper reports on the results of a study of hadronic events, with large visible energy, visible mass and transverse momentum, from the data collected by the L3 experiment at $\sqrt{s} = 161\text{--}172$ GeV. The idea here is to identify events with a Z decaying hadronically recoiling against missing energy and momentum due to undetected particles. If a particle is produced in association with the Z and decays into invisible particles, then a peak in the missing mass spectrum should be observed. The kinematic region investigated here is different from those investigated in other studies of hadronic events with missing energy and momentum, such as the one for the measurement of the $W\nu$ cross section [1] as well as the search for the Standard Model Higgs boson, H_{SM} , in the $ZH_{\text{SM}} \rightarrow \nu\bar{\nu}q\bar{q}$ channel [2] and supersymmetric particle searches [3].

Non-Standard Model processes could produce an unexpected excess of events in the spectrum of the missing mass recoiling to the Z. One example is the production of a non-minimal Higgs boson, h , decaying into invisible particles, in association with a hadronically decaying Z boson. Examples of invisible particles which a non-minimal Higgs could decay to are light neutralinos [4] in the context of supersymmetric extensions of the Standard Model; or Majorons [5], in so called Majoron models, used to generate neutrino masses.

2 Data and Monte Carlo samples

We use data corresponding to integrated luminosities of 10.8, 1.0 and 9.2 pb^{-1} collected by the L3 detector [6] at LEP at centre-of-mass energies, \sqrt{s} , of 161.3, 170.3 and 172.3 GeV, respectively. For the signal efficiency studies a sample of Higgs events has been generated using PYTHIA [7], imposing 100% decay branching fraction of the Higgs boson into invisible particles. About 3500 Higgs events, with hadronic Z decay, were simulated for each Higgs mass value investigated. The Standard Model cross section for Higgs production is calculated using the HZHA generator [8]. For the study of fermion pair and four-fermion productions the following Monte Carlo generators were used: PYTHIA ($e^+e^- \rightarrow q\bar{q}(\gamma)$), KORALW [9] ($e^+e^- \rightarrow W^+W^-$), PYTHIA and PHOJET [10] ($e^+e^- \rightarrow e^+e^-q\bar{q}$), and EXCALIBUR [11] ($e^+e^- \rightarrow f\bar{f}'f\bar{f}'$). The number of simulated fermion pair and four-fermion events corresponds to at least 100 times the collected luminosity.

The L3 detector response is simulated using the GEANT 3.15 [12] program, which takes into account the effect of energy loss, multiple scattering and showering in the detector. The GHEISHA [13] program is used to simulate hadronic interactions in the detector.

3 Event properties

Higgs events, produced via the Higgs-strahlung process $e^+e^- \rightarrow Zh$, with $Z \rightarrow q\bar{q}$ and $h \rightarrow$ invisible particles, and Standard Model Higgs events, produced via the same process, $e^+e^- \rightarrow ZH_{\text{SM}}$, with $Z \rightarrow \nu\bar{\nu}$ and $H_{\text{SM}} \rightarrow q\bar{q}$, have similar signature: large visible energy, two acoplanar hadronic jets, large transverse momentum and absence of isolated leptons.

However, at present centre-of-mass energies, the Z boson is produced almost at rest, thus for invisibly decaying Higgs events the visible energy and visible mass are close to the Z mass, independently of the Higgs mass. This is not the case for Standard Model Higgs events, where the visible energy and visible masses are generally below the Z mass (in the Higgs mass range investigated at present energies), and depend upon the Higgs mass. Furthermore, b-tagging is not as efficient in selecting invisibly decaying Higgs events as in the Standard Model Higgs search, since only about 15% of the total number of Higgs events will contain a $b\bar{b}$ pair (from the Z) as compared to about 87% of the total Standard Model Higgs events. Thus the analysis is based only on kinematic cuts and does not make use of b-tagging.

Hadronic events with large visible energy and momentum also originate from Standard Model processes, such as quark pair production ($e^+e^- \rightarrow q\bar{q}(\gamma)$) and four-fermion production, involving charged gauge boson exchange (W^+W^- and $We\nu$ production) and neutral gauge boson exchange ($Z/\gamma^*Z/\gamma^*$ and Zee production). The missing energy and momentum in these events is either genuine (e.g. in W^+W^- events, when one W decays into lepton+neutrino) or results from energy mis-measurement and incomplete detector coverage. The most important sources of background in this search are $q\bar{q}(\gamma)$, W^+W^- and $We\nu$ events. The first two have a relatively large production cross section (129 pb and 12.3 pb respectively for $q\bar{q}(\gamma)$ and W^+W^- cross sections at 172 GeV), while the third, despite its relatively small production cross section (0.35 and 0.45 pb at 161 and 172 GeV respectively), gives a relatively large contribution in the same kinematic region as the Higgs signal.

4 Event selection

First we select hadronic events with large visible energy, small longitudinal imbalance, and small energy in the forward calorimeters to suppress the two-photon contribution $e^+e^- \rightarrow e^+e^-q\bar{q}$ and reduce the $q\bar{q}(\gamma)$ contribution, when the photon is in the forward region of the detector or escapes in the beam pipe. Then we apply additional requirements to further reduce the $q\bar{q}(\gamma)$ and W^+W^- contributions and select events with visible energy, momentum and mass consistent with a Z decaying into hadrons and recoiling against undetected particle. As we reduce the event sample we compare the observed spectra of the visible mass, calculated from the visible energy E_{vis} and momentum P_{vis} , $M_{\text{vis}} = (E_{\text{vis}}^2 - P_{\text{vis}}^2)^{1/2}$ and the missing mass $M_{\text{mis}} = (s + M_{\text{vis}}^2 - 2\sqrt{s}E_{\text{vis}})^{1/2}$, to the contributions from Standard Model fermion pair and four-fermion productions.

The quantities used in the selection are as follows: number of tracks, N_T ; number of calorimetric clusters, N_C ; the visible energy, E_{vis}/\sqrt{s} ; longitudinal and transverse imbalances, $|P_{\parallel}|/E_{\text{vis}}$ and P_{\perp}/E_{vis} , respectively; the total energy deposition in the electromagnetic calorimeter, E_{em} ; energy deposition in the luminosity monitor, E_{v4} ; energy deposition in the forward lead-scintillator calorimeter, E_{v8} ; the relative energy in a cone of 30° around the beam direction, $E_{\text{v30}}/E_{\text{vis}}$; the larger of the two jet masses, $\max(M_{j1}, M_{j2})$, when the event is forced into two jets using DURHAM algorithm [14]; the sum of the angles between

the jets, θ_{123} , when the event is forced into three jets using the DURHAM algorithm; the energy deposition in $\pm 25^\circ$ of the missing momentum direction in the plane transverse to the beam, E_{25}^\perp ; the number of high energy isolated leptons, $N_{i\ell}$, i.e. leptons (e, μ, τ) with energy $E_\ell > 5$ GeV and isolation $I_\ell < 1$ GeV, where I_ℓ is the energy deposition in the region between 10° and 30° half opening angle around the lepton direction.

The following cuts are applied in order to reduce the Standard Model contributions, mainly from $q\bar{q}(\gamma)$ and W^+W^- productions:

- 1) Hadronic preselection: $N_C > 14$, $N_T > 4$, $E_{\text{em}} > 10$ GeV, $E_{v4} < 5$ GeV, $E_{v8} < 10$ GeV, $0.4 < E_{\text{vis}}/\sqrt{s} < 1$, $|P_{\parallel}|/E_{\text{vis}} < 0.5$;
- 2) $E_{v30}/E_{\text{vis}} < 0.5$;
- 3) $E_{\text{vis}}/\sqrt{s} < 0.7$;
- 4) $|P_{\parallel}|/E_{\text{vis}} < 0.3$;
- 5) $\max(M_{j1}, M_{j2}) < 40$ GeV;
- 6) $\theta_{123} < 349^\circ$ for $\sqrt{s} = 172$ GeV or $\theta_{123} < 355^\circ$ for $\sqrt{s} = 161$ GeV;
- 7) $P_{\perp}/E_{\text{vis}} > 0.1$;
- 8) $N_{i\ell} = 0$ and $E_{25}^\perp < 12$ GeV.

The distributions of the transverse imbalance, the maximum jet mass, the visible mass and the missing mass are shown in Figures 1(a) through 1(d) after the hadronic preselection (cut 1), for the data, the Standard Model expectation and, for comparison, a 70 GeV Higgs signal at $\sqrt{s} = 172$ GeV. At this centre-of-mass energy, after the hadronic preselection, 554 events are observed in the data, while 564 events are expected from Standard Model processes: 83% from $q\bar{q}\gamma$ production, 16% from W^+W^- production and the remaining 1% from $W\nu$, Zee and $Z/\gamma^*Z/\gamma^*$ production. At $\sqrt{s} = 161$ GeV 791 events are observed with 778 expected from Standard Model processes: 96% from $q\bar{q}\gamma$, 3% from W^+W^- , and 1% from $W\nu$, Zee, and $Z/\gamma^*Z/\gamma^*$ production. The Higgs signal efficiency is 95%: 5.1 Higgs events are expected at 172 GeV and 1.2 at 161 GeV, for 70 GeV Higgs mass, assuming Standard Model cross section for Higgs production via $e^+e^- \rightarrow Zh$ process.

The selection progressively reduces the $q\bar{q}(\gamma)$ contribution and to a lesser extent the W^+W^- and $W\nu$ contributions. The most effective requirements to reduce the latter are the jet mass cut (cut 5), the θ_{123} angle cut (cut 6), the absence of isolated high energy leptons and the isolation of the missing energy (cut 8). The jet mass cut and the θ_{123} angle cut, in particular, are very effective at reducing the W^+W^- contribution when one W decays hadronically and the other into a neutrino plus a tau. If the tau is not identified, it is included in one of the two jets when the event is reconstructed into two jets. Thus one of the two jet masses is high compared to genuine two-jet events. Similarly, when the $q\bar{q}\tau\nu$ event is reconstructed into three jets it is likely to have a value of θ_{123} larger than for a genuine two-jet event.

The number of events observed, after sequentially applying the selection cuts, compared to the expected Standard Model contributions, is shown in Fig. 2. Good agreement between the data and the Standard Model expectation is found in the subsequent steps of the selection. For comparison, the number of events expected for two invisible Higgs masses, assuming Standard Model Higgs production cross section, is also given in Fig. 2.

In Fig. 3 the distributions of M_{vis} and M_{mis} , after selection cuts 1 through 6, are shown at centre-of-mass energies of 161 and 172 GeV. At this stage of the analysis, at $\sqrt{s} = 172$ GeV 21 events are observed in the data, while 20.7 events are expected from Standard Model processes: 47% from $q\bar{q}\gamma$ events, 48% from W^+W^- events and 5% from Zee, $Z/\gamma^*Z/\gamma^*$ and $W\nu$ events. At $\sqrt{s} = 161$ GeV 35 events are observed with 25.1 expected from Standard Model processes: 81% from $q\bar{q}\gamma$, 13% from W^+W^- , and 6% from Zee, $Z/\gamma^*Z/\gamma^*$ and $W\nu$ production. At this stage of the selection, the Higgs signal efficiency is 63% for a 65 GeV Higgs at $\sqrt{s}=161$ GeV and 62% for a 70 GeV Higgs at $\sqrt{s}=172$ GeV.

For the Higgs events, the visible mass is centered about the Z mass, with a Z mass resolution σ_Z of about 9 GeV, and the missing mass is centered about the Higgs mass, with a resolution which ranges from 15 to 12 GeV for Higgs masses between 60 and 70 GeV at $\sqrt{s} = 172$ GeV. A better resolution in the Higgs mass is obtained by imposing the constraint that the visible energy and momentum comes from the Z decay, and determining the Higgs energy from rescaling the measured missing energy, imposing total energy and momentum constraints. The expression for the reconstructed Higgs mass, M_{rh} , is

$$M_{\text{rh}} = \frac{\sqrt{s} - [s - (s - (M'_Z)^2)(1 - \beta_{\text{mis}}^2)]^{1/2}}{[1 - \beta_{\text{mis}}^2]^{1/2}}.$$

Here $\beta_{\text{mis}} = P_{\text{vis}}/(\sqrt{s} - E_{\text{vis}})$ is, in the Higgs events, the measured Higgs velocity. The quantity $M'_Z = M_Z + (M_{\text{vis}} - M_Z)\Gamma_Z/\sigma_Z$ is used rather than the Z mass, M_Z , to take into account the finite Z width, Γ_Z . The resolution of M_{rh} ranges from 5.9 GeV for a 60 GeV Higgs to 3.6 GeV for a 70 GeV Higgs [15] at $\sqrt{s}=172$ GeV.

5 Results and conclusions

The distributions of M_{vis} , M_{mis} and M_{rh} , after applying final selection (cuts 1 through 8), are shown in Fig. 4 for the data and the Standard Model contributions. Also shown (dashed histogram) is the expected contribution from a 70 (65) GeV Higgs at $\sqrt{s} = 172$ (161) GeV, normalised to the actual luminosity using the Standard Model Higgs production cross section, added to the contributions from Standard Model processes. The values of M_{vis} , M_{mis} and M_{rh} for the data events surviving the final selection are given in Table 1. No significant excess over the expected Standard Model contributions is observed in the measured mass distributions.

The observed number of events and the expected contributions from Standard Model processes are compared in Table 2 after final selection. In total we expect 3.4 ± 0.4 and 6.0 ± 0.6 events from Standard Model physics processes and we observe 3 and 5 events at $\sqrt{s} = 161$ and 172 GeV, respectively. The error on the Standard Model expectation

Observed event	$M_{\text{vis}}(\text{GeV})$	$M_{\text{mis}}(\text{GeV})$	$M_{\text{rh}}(\text{GeV})$
$\sqrt{s}=172 \text{ GeV}$			
# 1	72 ± 9	62 ± 9	50 ± 4
# 2	80 ± 8	57 ± 9	50 ± 4
# 3	71 ± 9	79 ± 8	61 ± 4
# 4	82 ± 8	82 ± 8	72 ± 3
# 5	82 ± 8	80 ± 8	70 ± 3
$\sqrt{s}=161 \text{ GeV}$			
# 1	89 ± 9	< 4	< 4
# 2	73 ± 9	79 ± 8	60 ± 4
# 3	81 ± 8	75 ± 8	64 ± 4

Table 1: The values of the visible mass, the missing mass and the reconstructed Higgs mass for the data events passing the final selection.

SM processes	$\sqrt{s}=161 \text{ GeV}$	$\sqrt{s}=172 \text{ GeV}$
$q\bar{q}$	1.15 ± 0.13	0.32 ± 0.06
Zee	0.003 ± 0.002	0.003 ± 0.002
$Z/\gamma^*Z/\gamma^*$	0.028 ± 0.007	0.053 ± 0.005
$We\nu$	0.90 ± 0.05	0.68 ± 0.07
W^+W^-	1.34 ± 0.06	5.02 ± 0.11
Total expected	$3.40 \pm 0.15(stat)$	$6.00 \pm 0.15(stat)$
Total observed	3	5

Table 2: The number of events observed after final selection in the data collected at centre-of-mass energies between 161 and 172 GeV, compared to the number of expected events from Standard Model processes. The quoted errors on the Monte Carlo expectations are statistical only. The systematic errors are discussed in the text.

includes the error from limited Monte Carlo statistics, which amounts to 4% (see Table 2), and the error on the selection efficiency. The latter is mainly due to energy calibration uncertainties and it has been estimated by repeating the analysis with the global energy scale changed by $\pm 3\%$ and the energy scales of the individual subdetectors by $\pm 5\%$ [2]. Thus, a total error of about 10% is estimated to affect the Standard Model expectation.

Efficiencies to select $e^+e^- \rightarrow Zh$ events, with $Z \rightarrow q\bar{q}$ and $h \rightarrow$ invisible particles, at $\sqrt{s}=161$ and 172 GeV, are given in Table 3 for several Higgs masses. The total error affecting these efficiencies is at most 4%, including both the effect of the limited Monte Carlo statistics (contributing up to 2%) and that of the energy calibration uncertainties (contributing between 2.5 and 3.5%, depending on the Higgs mass).

Since no signal is observed an upper limit is set on the invisible decay rate of a non-minimal Higgs boson. The limit is derived from the present results combined with the

	$\sqrt{s} \approx 91$ GeV		$\sqrt{s}=161$ GeV		$\sqrt{s}=172$ GeV	
Higgs mass (GeV)	$\epsilon_{Zh}(\%)$	N	$\epsilon_{Zh}(\%)$	N	$\epsilon_{Zh}(\%)$	N
50	39	47.5	47	5.87	43	4.53
60	38	11.4	48	3.77	46	3.70
65	36	4.55	42	2.10	47	3.15
67	35	2.99	37	1.36	48	2.94
69	33	1.87	29	0.581	45	2.48
70	32	1.46	28	0.362	46	2.40
71	31	1.12	27	0.230	45	2.11
73	30	0.64	24	0.100	45	1.87

Table 3: Efficiencies, ϵ_{Zh} , and corresponding number of expected events, N , after selection, for the Zh signal, assuming the Zh production cross section to be the same as for the Standard Model Higgs and decay branching fraction into invisible particles to be 100%. The efficiencies for $\sqrt{s}=161$ -172 GeV are affected by a 4% total uncertainty and for LEP1 they are affected by a 3% total uncertainty.

L3 results from LEP1 [17]. No invisibly decaying Higgs candidates were selected from the data collected at the Z resonance. The signal efficiencies at $\sqrt{s} \approx 91$ GeV are reported in Table 3. The total error affecting these efficiencies is 3%. The number of signal events expected at the three center-of-mass energies, calculated assuming the Zh production cross-section to be the same as for the Standard Model Higgs boson and the branching fraction into invisible final states to be 100%, is also given in Table 3.

A confidence level calculation, which includes the errors on signal and background expectations, is done according to the method proposed in Ref. [16]. The M_{rh} distributions (see Fig. 4(c) and (f)) for the data, the Standard Model background and the Higgs signal, for several Higgs mass values, are used in the calculation of the confidence level. Combining the 161-172 GeV results with those from LEP1, a lower limit (Fig. 5(a)) is set on the mass of an invisibly decaying Higgs boson at 95% confidence level

$$m_h > 69.6 \text{ GeV},$$

assuming that the Higgs production cross section $\sigma(Zh)$ is the same as for the Standard Model Higgs and the Higgs branching fraction into invisible particles, $BR(h \rightarrow \text{invisible particles})$, is 100%.

The $e^+e^- \rightarrow Zh$ production cross section and the branching fraction into visible and invisible final states of a non-minimal Higgs boson h are model dependent. Thus we set an experimental upper limit on the rate of invisible Higgs final states, relative to the Standard Model Higgs rate, $R_{inv} = \sigma(Zh)BR(h \rightarrow \text{invisible particles})/\sigma(ZH_{SM})$, as a function of the Higgs mass. This limit, which can be used to bound the parameter space of the different models predicting invisible Higgs decays, is shown in Fig. 5(b) for Higgs masses above 50 GeV, where the 161-172 GeV results improve the LEP1 limit on R_{inv} . The hatched area in Fig. 5(b) is excluded at 95% confidence level.

In conclusion, these results improve on those obtained in previous analyses at LEP1 [17, 18, 19] and are the first ones reported at $\sqrt{s}=161\text{-}172$ GeV concerning invisible Higgs decays.

Acknowledgements

We wish to express our gratitude to the CERN Accelerator Divisions for the good performance of the LEP machine. We acknowledge the efforts of the engineers and technicians who have participated in the construction and the maintenance of this experiment.

References

- [1] L3 Collaboration, M. Acciarri *et al.*, “Production of Single W Bosons at LEP” , CERN-PPE/97-28, submitted to Phys. Lett. B.
- [2] L3 Collaboration, M. Acciarri *et al.*, “Search for the Standard Model Higgs Boson in e^+e^- collisions at $161 \leq \sqrt{s} \leq 172$ GeV”, submitted to Phys. Lett. B.
- [3] L3 Collaboration, M. Acciarri *et al.*, “Searches for Charginos, Neutralinos and Sleptons at $\sqrt{s}=161$ -172 GeV”, in preparation.
- [4] K. Griest, H.E. Haber, Phys. Rev. **D 37** (1988) 719. A. Djouadi, P. Janot, J. Kalinowski, P.M. Zerwas, Phys. Lett. **B 376** (1996) 220.
- [5] A.S. Joshipura, J.W.F. Valle, Nucl. Phys. **B 397** (1993) 105;
F. de Campos, O.J. Eboli, J. Rosiek, J.W.F. Valle, Phys. Rev. **D 55** (1997) 1316.
- [6] L3 Collaboration, B. Adeva *et al.*, Nucl.Instr.Meth. **A289** (1990) 35; J.A. Bakken *et al.*, Nucl.Instr.Meth. **A275** (1989) 81; O. Adriani *et al.*, Nucl.Instr.Meth. **A302** (1991) 53; B. Adeva *et al.*, Nucl.Instr.Meth. **A323** (1992) 109; K. Deiters *et al.*, Nucl.Instr.Meth. **A323** (1992) 162; M. Chemarin *et al.*, Nucl.Instr.Meth. **A349** (1994) 345; B. Acciari *et al.*, Nucl.Instr.Meth. **A351** (1994) 300; G. Basti *et al.*, Nucl.Instr.Meth. **A374** (1996) 293; A. Adam *et al.*, Nucl.Instr.Meth. **A383** (1996) 342.
- [7] T. Sjöstrand, CERN-TH/7112/93 (1993), revised August 1995; T. Sjöstrand, Comp.Phys.Comm. 82 (1994) 74.
- [8] P. Janot, “The HZHA generator”, in “Physics at LEP2”, Eds. G. Altarelli, T. Sjöstrand and F. Zwirner, CERN 96-01 (1996) Vol.2, 309.
- [9] M. Skrzypek *et al.*, Comp. Phys. Comm. **94** (1996) 216; M. Skrzypek *et al.*, Phys. Lett. **B372** (1996) 289.
- [10] R. Engel, Z. Phys. **C66** (1995) 203; R. Engel, J. Ranft and S. Roesler, Phys. Rev. **D52** (1995) 1459.
- [11] F.A. Berends, R. Kleiss and R. Pittau, Nucl. Phys. **B 424** (1994) 308; Nucl. Phys. **B 426** (1994) 344; Nucl. Phys. (Proc. Suppl.) **B 37** (1994) 163; Phys. Lett. **B 335** (1994) 490; R. Kleiss and R. Pittau, Comp. Phys. Comm. **83** (1994) 14.
- [12] R. Brun *et al.*, preprint CERN DD/EE/84-1 (Revised 1987).
- [13] H. Fesefeldt, RWTH Aachen Report PITHA 85/02 (1985).
- [14] S. Catani *et al.*, Phys. Lett. **B 263** (1991) 491; S. Bethke *et al.*, Nucl.Phys. **B 370** (1992) 310.

- [15] M. Felcini, L3 Higgs Working Group, L3 internal note 2073, March 97 ¹⁾.
- [16] V.F. Obvatsov, Nucl. Instr. Meth. **A 316** (1993) 388.
- [17] L3 Collaboration, M. Acciarri *et al.*, Phys. Lett. **B 385** (1996) 454.
- [18] OPAL Collaboration, G. Alexander *et al.*, Phys. Lett. **B 377** (1996) 273.
- [19] ALEPH Collaboration, D. Buskulic *et al.*, Phys. Lett. **B 313** (1993) 549.

¹⁾This L3 Note is freely available on request from: The L3 secretariat, CERN, CH-1211 Geneva 23, Switzerland. Internet: <http://hpl3sn02.cern.ch/l3pubanddoc.html>

The L3 Collaboration:

M. Acciarri,²⁸ O. Adriani,¹⁷ M. Aguilar-Benitez,²⁷ S. Ahlen,¹¹ J. Alcaraz,²⁷ G. Alemanni,²³ J. Allaby,¹⁸ A. Aloisio,³⁰ G. Alverson,¹² M.G. Alvigi,³⁰ G. Ambrosi,²⁰ H. Anderhub,⁵⁰ V.P. Andreev,³⁹ T. Angelescu,¹³ F. Anselmo,⁹ A. Arefiev,²⁹ T. Azemoon,³ T. Aziz,¹⁰ P. Bagnaia,³⁸ L. Baksay,⁴⁵ R.C. Ball,³ S. Banerjee,¹⁰ Sw. Banerjee,¹⁰ K. Banic,⁴⁷ A. Barczyk,^{50,48} R. Barillere,¹⁸ L. Barone,³⁸ P. Bartolini,³⁵ A. Baschirotto,²⁸ M. Basile,⁹ R. Battiston,³⁵ A. Bay,²³ F. Becattini,¹⁷ U. Becker,¹⁶ F. Behner,⁵⁰ J. Berdugo,²⁷ P. Berges,¹⁶ B. Bertucci,³⁵ B.L. Betev,⁵⁰ S. Bhattacharya,¹⁰ M. Biasini,¹⁸ A. Biland,⁵⁰ G.M. Bilei,³⁵ J.J. Blaising,⁴ S.C. Blyth,³⁶ G.J. Bobbink,² R. Bock,¹ A. Böhm,¹ L. Boldizsar,¹⁴ B. Borgia,³⁸ D. Bourilkov,⁵⁰ M. Bourquin,²⁰ D. Boutigny,⁴ S. Braccini,²⁰ J.G. Branson,⁴¹ V. Brigljevic,⁵⁰ I.C. Brock,³⁶ A. Buffini,¹⁷ A. Buijs,⁴⁶ J.D. Burger,¹⁶ W.J. Burger,²⁰ J. Busenitz,⁴⁵ X.D. Cai,¹⁶ M. Campanelli,⁵⁰ M. Capell,¹⁶ G. Cara Romeo,⁹ G. Carlino,³⁰ A.M. Cartacci,¹⁷ J. Casaus,²⁷ G. Castellini,¹⁷ F. Cavallari,³⁸ N. Cavallo,³⁰ C. Cecchi,²⁰ M. Cerrada,²⁷ F. Cesaroni,²⁴ M. Chamizo,²⁷ Y.H. Chang,⁵² U.K. Chaturvedi,¹⁹ S.V. Chekanov,³² M. Chemarin,²⁶ A. Chen,⁵² G. Chen,⁷ G.M. Chen,⁷ H.F. Chen,²¹ H.S. Chen,⁷ M. Chen,¹⁶ G. Chiefari,³⁰ C.Y. Chien,⁵ L. Cifarelli,⁴⁰ F. Cindolo,⁹ C. Civinini,¹⁷ I. Clare,¹⁶ R. Clare,¹⁶ H.O. Cohn,³³ G. Coignet,⁴ A.P. Colijn,² N. Colino,²⁷ V. Commichau,¹ S. Costantini,⁸ F. Cotorobai,¹³ B. de la Cruz,²⁷ A. Csilling,¹⁴ T.S. Dai,¹⁶ R.D. Alessandro,¹⁷ R. de Asmundis,³⁰ A. Degré,⁴ K. Deiters,⁴⁸ P. Denes,³⁷ F. DeNotaristefani,³⁸ D. DiBitonto,⁴⁵ M. Diemoz,³⁸ D. van Dierendonck,² F. Di Lodovico,⁵⁰ C. Dionisi,³⁸ M. Dittmar,⁵⁰ A. Dominguez,⁴¹ A. Doria,³⁰ M.T. Dova,^{19,4} E. Drago,³⁰ D. Duchesneau,⁴ P. Duinker,² I. Duran,⁴² S. Dutta,¹⁰ S. Easo,³⁵ Yu. Efremenko,³³ H. El Mamouni,²⁶ A. Engler,³⁶ F.J. Eppling,¹⁶ F.C. Erne,² J.P. Ernenwein,²⁶ P. Extermann,²⁰ M. Fabre,⁴⁸ R. Faccini,³⁸ S. Falciano,³⁸ A. Favara,¹⁷ J. Fay,²⁶ O. Fedin,³⁹ M. Felcini,⁵⁰ B. Fenyi,⁴⁵ T. Ferguson,³⁶ F. Ferroni,³⁸ H. Fesefeldt,¹ E. Fiandrin,³⁵ J.H. Field,²⁰ F. Filthaut,³⁶ P.H. Fisher,¹⁶ I. Fisk,⁴¹ G. Forconi,¹⁶ L. Fredj,²⁰ K. Freudenreich,⁵⁰ C. Furetta,²⁸ Yu. Galaktionov,^{29,16} S.N. Ganguli,¹⁰ P. Garcia-Abia,⁴⁹ S.S. Gau,¹² S. Gentile,³⁸ J. Gerald,⁵ N. Gheordanescu,¹³ S. Giagu,³⁸ S. Goldfarb,²³ J. Goldstein,¹¹ Z.F. Gong,²¹ A. Gougas,⁵ G. Gratta,³⁴ M.W. Gruenewald,⁸ V.K. Gupta,³⁷ A. Gurtu,¹⁰ L.J. Gutay,⁴⁷ B. Hartmann,¹ A. Hasan,³¹ D. Hatzifotiadiou,⁹ T. Hebbeker,⁸ A. Hervé,¹⁸ W.C. van Hoek,³² H. Hofer,⁵⁰ S.J. Hong,⁴⁴ H. Hoorani,³⁶ S.R. Hou,⁵² G. Hu,⁵ V. Innocente,¹⁸ K. Jenkes,¹ B.N. Jin,⁷ L.W. Jones,³ P. de Jong,¹⁸ I. Josa-Mutuberría,²⁷ A. Kasser,²³ R.A. Khan,¹⁹ D. Kamrad,⁴⁹ Yu. Kamyshev,³³ J.S. Kapustinsky,²⁵ Y. Karyotakis,⁴ M. Kaur,^{19,4} M.N. Kienzle-Focacci,²⁰ D. Kim,³⁸ D.H. Kim,⁴⁴ J.K. Kim,⁴⁴ S.C. Kim,⁴⁴ Y.G. Kim,⁴⁴ W.W. Kinnison,²⁵ A. Kirkby,³⁴ D. Kirkby,³⁴ J. Kirkby,¹⁸ D. Kiss,¹⁴ W. Kittel,³² A. Klimentov,^{16,29} A.C. König,³² A. Kopp,⁴⁹ I. Korolko,²⁹ V. Koutsenko,^{16,29} R.W. Kraemer,³⁶ W. Krenz,¹ A. Kunin,^{16,29} P. Ladron de Guevara,²⁷ G. Landi,¹⁷ C. Lapoint,¹⁶ K. Lassila-Perini,⁵⁰ P. Laurikainen,²² M. Lebeau,¹⁸ A. Lebedev,¹⁶ P. Lebrun,²⁶ P. Lecomte,⁵⁰ P. Lecoq,¹⁸ P. Le Coultre,⁵⁰ H. J. Lee,⁸ C. Leggett,³ J.M. Le Goff,¹⁸ R. Leiste,⁴⁹ E. Leonard,³⁸ P. Levchenko,³⁹ C. Li,²¹ C.H. Lin,⁵² W.T. Lin,⁵² F.L. Linde,^{2,18} L. Lista,³⁰ Z.A. Liu,⁷ W. Lohmann,⁴⁹ E. Longo,³⁸ W. Lu,³⁴ Y.S. Lu,⁷ K. Lübelmeyer,¹ C. Luci,³⁸ D. Luckey,¹⁶ L. Luminari,³⁸ W. Lustermaier,⁴⁸ W.G. Ma,²¹ M. Maity,¹⁰ G. Majumder,¹⁰ L. Malgeri,³⁸ A. Malinin,²⁹ C. Mañá,²⁷ D. Mangeol,³² S. Mangla,¹⁰ P. Marchesini,⁵⁰ A. Marin,¹¹ J.P. Martin,²⁶ F. Marzano,³⁸ G.G.G. Massaro,² D. McNally,¹⁸ S. Mele,³⁰ L. Merola,³⁰ M. Meschini,¹⁷ W.J. Metzger,³² M. von der Mey,¹ Y. Mi,²³ A. Mihul,¹³ A.J.W. van Mil,³² G. Mirabelli,³⁸ J. Mnich,¹⁸ P. Molnar,⁸ B. Monteleoni,¹⁷ R. Moore,³ S. Morganti,³⁸ T. Moulik,¹⁰ R. Mount,³⁴ S. Müller,¹ F. Muheim,²⁰ A.J.M. Muijs,² S. Nahn,¹⁶ M. Napolitano,³⁰ F. Nessi-Tedaldi,⁵⁰ H. Newman,³⁴ T. Niessen,¹ A. Nippe,¹ A. Nisati,³⁸ H. Nowak,⁴⁹ Y.D. Oh,⁴⁴ H. Opitez,¹ G. Organtini,³⁸ R. Ostonen,²² C. Palomares,²⁷ D. Pandoulas,¹ S. Paoletti,³⁸ P. Paolucci,³⁰ H.K. Park,³⁶ I.H. Park,⁴⁴ G. Pascale,³⁸ G. Passaleva,¹⁸ S. Patricelli,³⁰ T. Paul,¹² M. Pauluzzi,³⁵ C. Paus,¹⁸ F. Pauss,⁵⁰ D. Peach,¹⁸ Y.J. Pei,¹ S. Pensotti,²⁸ D. Perret-Gallix,⁴ B. Petersen,³² S. Petrak,⁸ A. Pevsner,⁵ D. Piccolo,³⁰ M. Pieri,¹⁷ P.A. Piroué,³⁷ E. Pistolesi,²⁸ V. Plyaskin,²⁹ M. Pohl,⁵⁰ V. Pojidaev,^{29,17} H. Postema,¹⁶ N. Produit,²⁰ D. Prokofiev,³⁹ G. Rahal-Callot,⁵⁰ N. Raja,¹⁰ P.G. Rancoita,²⁸ M. Rattaggi,²⁸ G. Raven,⁴¹ P. Razi,³¹ K. Read,³³ D. Ren,⁵⁰ M. Rescigno,³⁸ S. Reucroft,¹² T. van Rhee,⁴⁶ S. Riemann,⁴⁹ K. Riles,³ O. Rind,³ A. Robohm,⁵⁰ J. Rodin,¹⁶ B.P. Roe,³ L. Romero,²⁷ S. Rosier-Lees,⁴ Ph. Rosselet,²³ W. van Rossum,⁴⁶ S. Roth,¹ J.A. Rubio,¹⁸ D. Ruschmeier,⁸ H. Rykaczewski,⁵⁰ J. Salicio,¹⁸ E. Sanchez,²⁷ M.P. Sanders,³² M.E. Sarakinos,²² S. Sarkar,¹⁰ M. Sassowsky,¹ G. Sauvage,⁴ C. Schäfer,¹ V. Schegelsky,³⁹ S. Schmidt-Kaerst,¹ D. Schmitz,¹ P. Schmitz,¹ M. Schneegans,⁴ N. Scholz,⁵⁰ H. Schopper,⁵¹ D.J. Schotanus,³² J. Schwenke,¹ G. Schwing,¹ C. Sciacca,³⁰ D. Sciarmino,²⁰ L. Servoli,³⁵ S. Shevchenko,³⁴ N. Shivarov,⁴³ V. Shoutko,²⁹ J. Shukla,²⁵ E. Shumilov,²⁹ A. Shvorob,³⁴ T. Siedenbueg,¹ D. Son,⁴⁴ A. Sopczak,⁴⁹ V. Soulimov,³⁰ B. Smith,¹⁶ P. Spillantini,¹⁷ M. Steuer,¹⁶ D.P. Stickland,³⁷ H. Stone,³⁷ B. Stoyanov,⁴³ A. Straessner,¹ K. Strauch,¹⁵ K. Sudhakar,¹⁰ G. Sultanov,¹⁹ L.Z. Sun,²¹ G.F. Susinno,²⁰ H. Suter,⁵⁰ J.D. Swain,¹⁹ X.W. Tang,⁷ L. Tauscher,⁶ L. Taylor,¹² Samuel C.C. Ting,¹⁶ S.M. Ting,¹⁶ M. Tonutti,¹ S.C. Tonwar,¹⁰ J. Tóth,¹⁴ C. Tully,³⁷ H. Tuchscherer,⁴⁵ K.L. Tung,⁷ Y. Uchida,¹⁶ J. Ulbricht,⁵⁰ U. Uwer,¹⁸ E. Valente,³⁸ R.T. Van de Walle,³² G. Vesztegombi,¹⁴ I. Vetlitsky,²⁹ G. Viertel,⁵⁰ M. Vivargent,⁴ R. Völckert,⁴⁹ H. Vogel,³⁶ H. Vogt,⁴⁹ I. Vorobiev,^{18,29} A.A. Vorobyov,³⁹ A. Vorvolakos,³¹ M. Wadhwa,⁶ W. Wallraff,¹ J.C. Wang,¹⁶ X.L. Wang,²¹ Z.M. Wang,²¹ A. Weber,¹ F. Wittgenstein,¹⁸ S.X. Wu,¹⁹ S. Wynnhoff,¹ J. Xu,¹¹ Z.Z. Xu,²¹ B.Z. Yang,²¹ C.G. Yang,⁷ X.Y. Yao,⁷ J.B. Ye,²¹ S.C. Yeh,⁵² J.M. You,³⁶ An. Zalite,³⁹ Yu. Zalite,³⁹ P. Zemp,⁵⁰ Y. Zeng,¹ Z. Zhang,⁷ Z.P. Zhang,²¹ B. Zhou,¹¹ Y. Zhou,³ G.Y. Zhu,⁷ R.Y. Zhu,³⁴ A. Zichichi,^{9,18,19} F. Ziegler.⁴⁹

- 1 I. Physikalisches Institut, RWTH, D-52056 Aachen, FRG[§]
- III. Physikalisches Institut, RWTH, D-52056 Aachen, FRG[§]
- 2 National Institute for High Energy Physics, NIKHEF, and University of Amsterdam, NL-1009 DB Amsterdam, The Netherlands
- 3 University of Michigan, Ann Arbor, MI 48109, USA
- 4 Laboratoire d'Annecy-le-Vieux de Physique des Particules, LAPP, IN2P3-CNRS, BP 110, F-74941 Annecy-le-Vieux CEDEX, France
- 5 Johns Hopkins University, Baltimore, MD 21218, USA
- 6 Institute of Physics, University of Basel, CH-4056 Basel, Switzerland
- 7 Institute of High Energy Physics, IHEP, 100039 Beijing, China[△]
- 8 Humboldt University, D-10099 Berlin, FRG[§]
- 9 University of Bologna and INFN-Sezione di Bologna, I-40126 Bologna, Italy
- 10 Tata Institute of Fundamental Research, Bombay 400 005, India
- 11 Boston University, Boston, MA 02215, USA
- 12 Northeastern University, Boston, MA 02115, USA
- 13 Institute of Atomic Physics and University of Bucharest, R-76900 Bucharest, Romania
- 14 Central Research Institute for Physics of the Hungarian Academy of Sciences, H-1525 Budapest 114, Hungary[†]
- 15 Harvard University, Cambridge, MA 02139, USA
- 16 Massachusetts Institute of Technology, Cambridge, MA 02139, USA
- 17 INFN Sezione di Firenze and University of Florence, I-50125 Florence, Italy
- 18 European Laboratory for Particle Physics, CERN, CH-1211 Geneva 23, Switzerland
- 19 World Laboratory, FBLJA Project, CH-1211 Geneva 23, Switzerland
- 20 University of Geneva, CH-1211 Geneva 4, Switzerland
- 21 Chinese University of Science and Technology, USTC, Hefei, Anhui 230 029, China[△]
- 22 SEFT, Research Institute for High Energy Physics, P.O. Box 9, SF-00014 Helsinki, Finland
- 23 University of Lausanne, CH-1015 Lausanne, Switzerland
- 24 INFN-Sezione di Lecce and Università Degli Studi di Lecce, I-73100 Lecce, Italy
- 25 Los Alamos National Laboratory, Los Alamos, NM 87544, USA
- 26 Institut de Physique Nucléaire de Lyon, IN2P3-CNRS, Université Claude Bernard, F-69622 Villeurbanne, France
- 27 Centro de Investigaciones Energeticas, Medioambientales y Tecnologicas, CIEMAT, E-28040 Madrid, Spain[‡]
- 28 INFN-Sezione di Milano, I-20133 Milan, Italy
- 29 Institute of Theoretical and Experimental Physics, ITEP, Moscow, Russia
- 30 INFN-Sezione di Napoli and University of Naples, I-80125 Naples, Italy
- 31 Department of Natural Sciences, University of Cyprus, Nicosia, Cyprus
- 32 University of Nijmegen and NIKHEF, NL-6525 ED Nijmegen, The Netherlands
- 33 Oak Ridge National Laboratory, Oak Ridge, TN 37831, USA
- 34 California Institute of Technology, Pasadena, CA 91125, USA
- 35 INFN-Sezione di Perugia and Università Degli Studi di Perugia, I-06100 Perugia, Italy
- 36 Carnegie Mellon University, Pittsburgh, PA 15213, USA
- 37 Princeton University, Princeton, NJ 08544, USA
- 38 INFN-Sezione di Roma and University of Rome, "La Sapienza", I-00185 Rome, Italy
- 39 Nuclear Physics Institute, St. Petersburg, Russia
- 40 University and INFN, Salerno, I-84100 Salerno, Italy
- 41 University of California, San Diego, CA 92093, USA
- 42 Dept. de Fisica de Partículas Elementales, Univ. de Santiago, E-15706 Santiago de Compostela, Spain
- 43 Bulgarian Academy of Sciences, Central Lab. of Mechatronics and Instrumentation, BU-1113 Sofia, Bulgaria
- 44 Center for High Energy Physics, Korea Adv. Inst. of Sciences and Technology, 305-701 Taejeon, Republic of Korea
- 45 University of Alabama, Tuscaloosa, AL 35486, USA
- 46 Utrecht University and NIKHEF, NL-3584 CB Utrecht, The Netherlands
- 47 Purdue University, West Lafayette, IN 47907, USA
- 48 Paul Scherrer Institut, PSI, CH-5232 Villigen, Switzerland
- 49 DESY-Institut für Hochenergiephysik, D-15738 Zeuthen, FRG

- 50 Eidgenössische Technische Hochschule, ETH Zürich, CH-8093 Zürich, Switzerland
- 51 University of Hamburg, D-22761 Hamburg, FRG
- 52 High Energy Physics Group, Taiwan, China
 - § Supported by the German Bundesministerium für Bildung, Wissenschaft, Forschung und Technologie
 - ‡ Supported by the Hungarian OTKA fund under contract numbers T14459 and T24011.
 - ‡ Supported also by the Comisión Interministerial de Ciencia y Tecnología
 - # Also supported by CONICET and Universidad Nacional de La Plata, CC 67, 1900 La Plata, Argentina
 - ◇ Also supported by Panjab University, Chandigarh-160014, India
 - △ Supported by the National Natural Science Foundation of China.

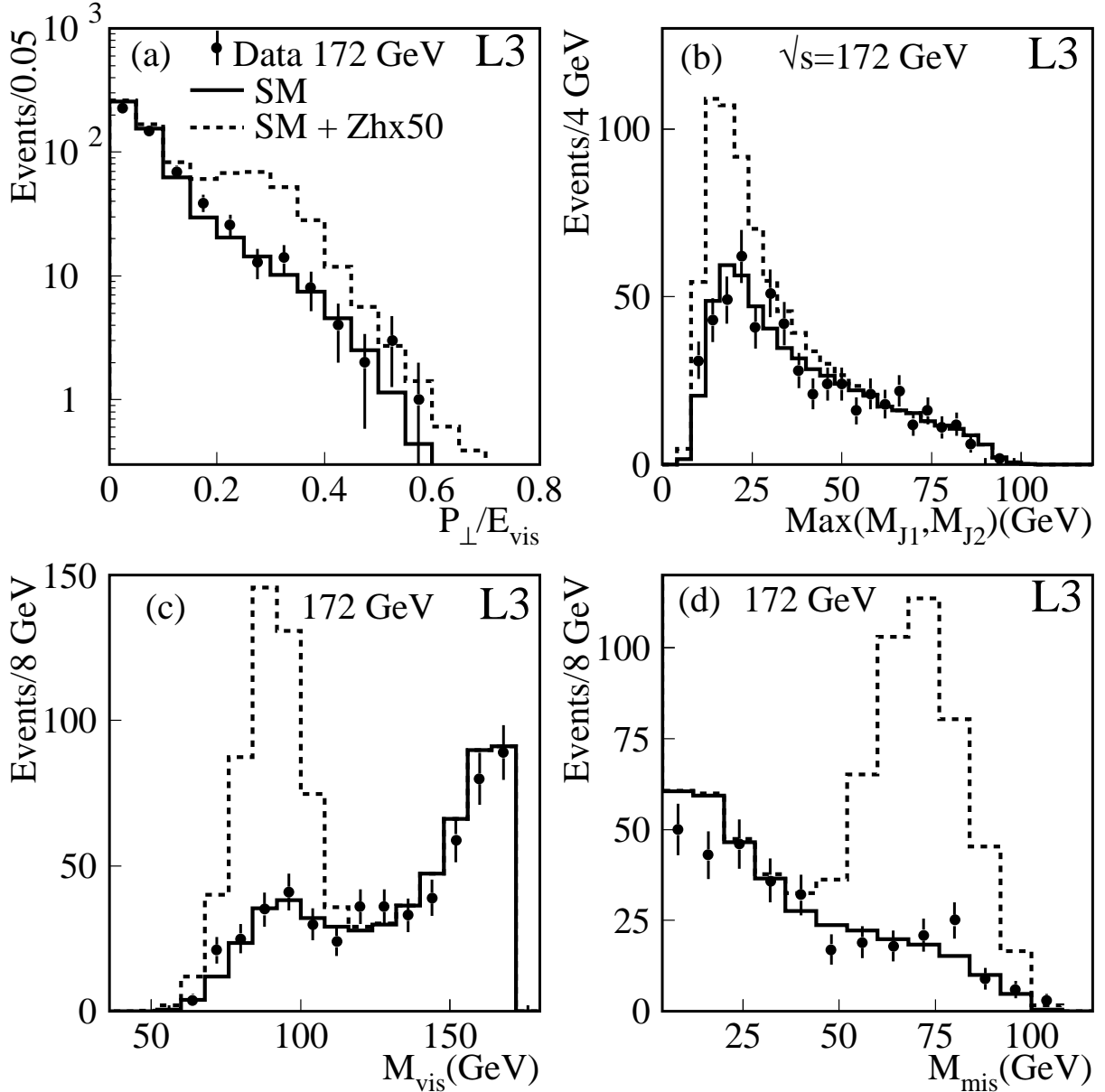


Figure 1: Distributions, at $\sqrt{s} = 172$ GeV, after the hadronic preselection (see text) of (a) the transverse imbalance, (b) the maximum jet mass, when the event is reconstructed into two jets, (c) the visible mass and (d) the missing mass. In (d) only events with $M_{\text{mis}}^2 \geq 16 \text{ GeV}^2$ are shown. The data (dots) are compared to the sum of the Standard Model contributions (solid histogram) from fermion pair production plus four fermion production. The sum of the Standard Model (SM) and the Higgs signal (Zh) contributions for a 70 GeV Higgs is shown by the dashed histogram. The Higgs contribution is normalised to 50 times the actual luminosity, using the Standard Model Higgs production cross section.

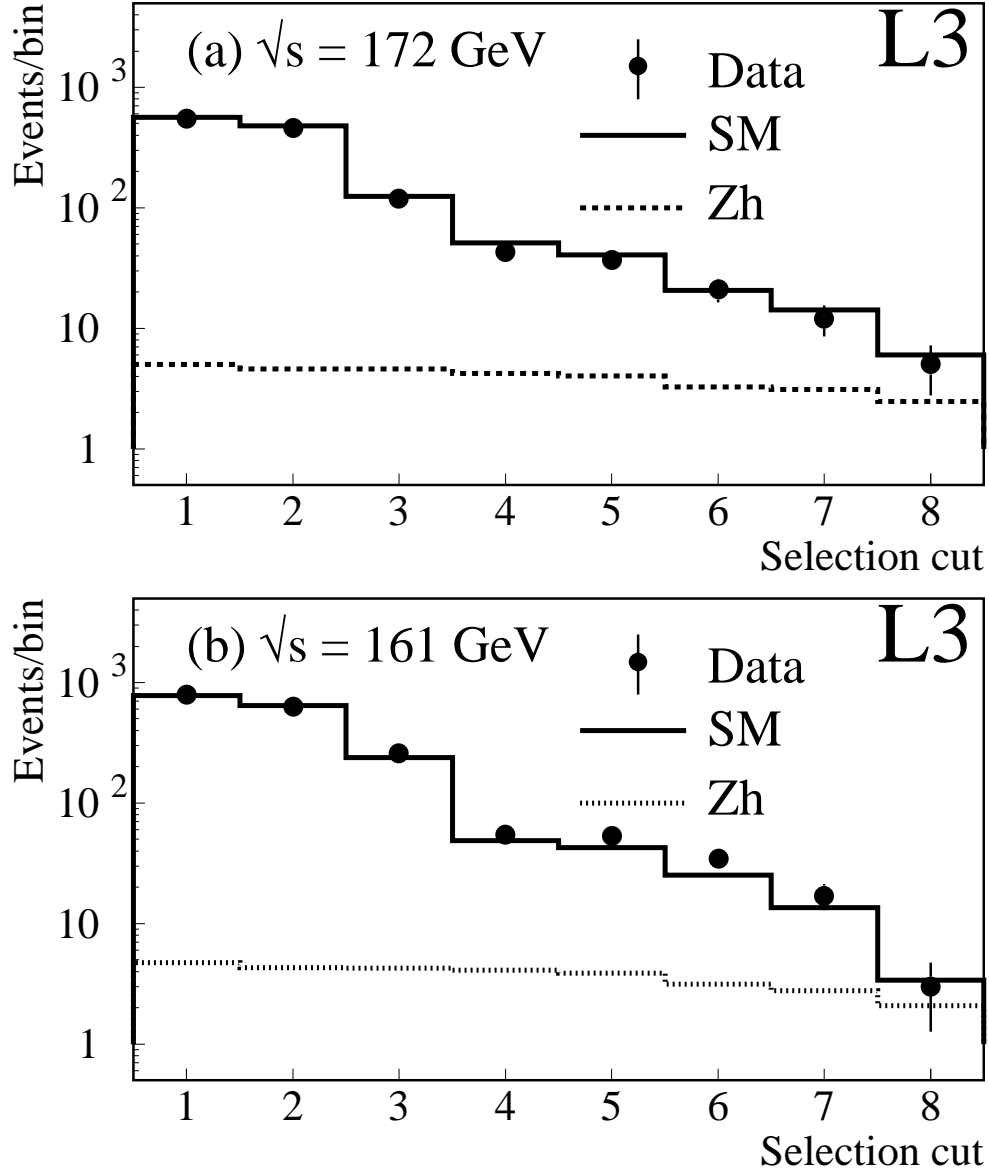


Figure 2: The number of events observed in the data (dots), after sequentially applying the selection cuts, at (a) $\sqrt{s} = 172$ GeV and (b) $\sqrt{s} = 161$ GeV, compared to the expectations for Standard Model production of fermion pairs plus four fermion final states (solid histogram). Superimposed is the number of events expected for a 70 (65) GeV Higgs signal, shown by the dashed (dotted) histogram, at $\sqrt{s} = 172$ (161) GeV. The Higgs distributions are normalised to the actual luminosities at the two centre-of-mass energies using the Standard Model Higgs production cross section.

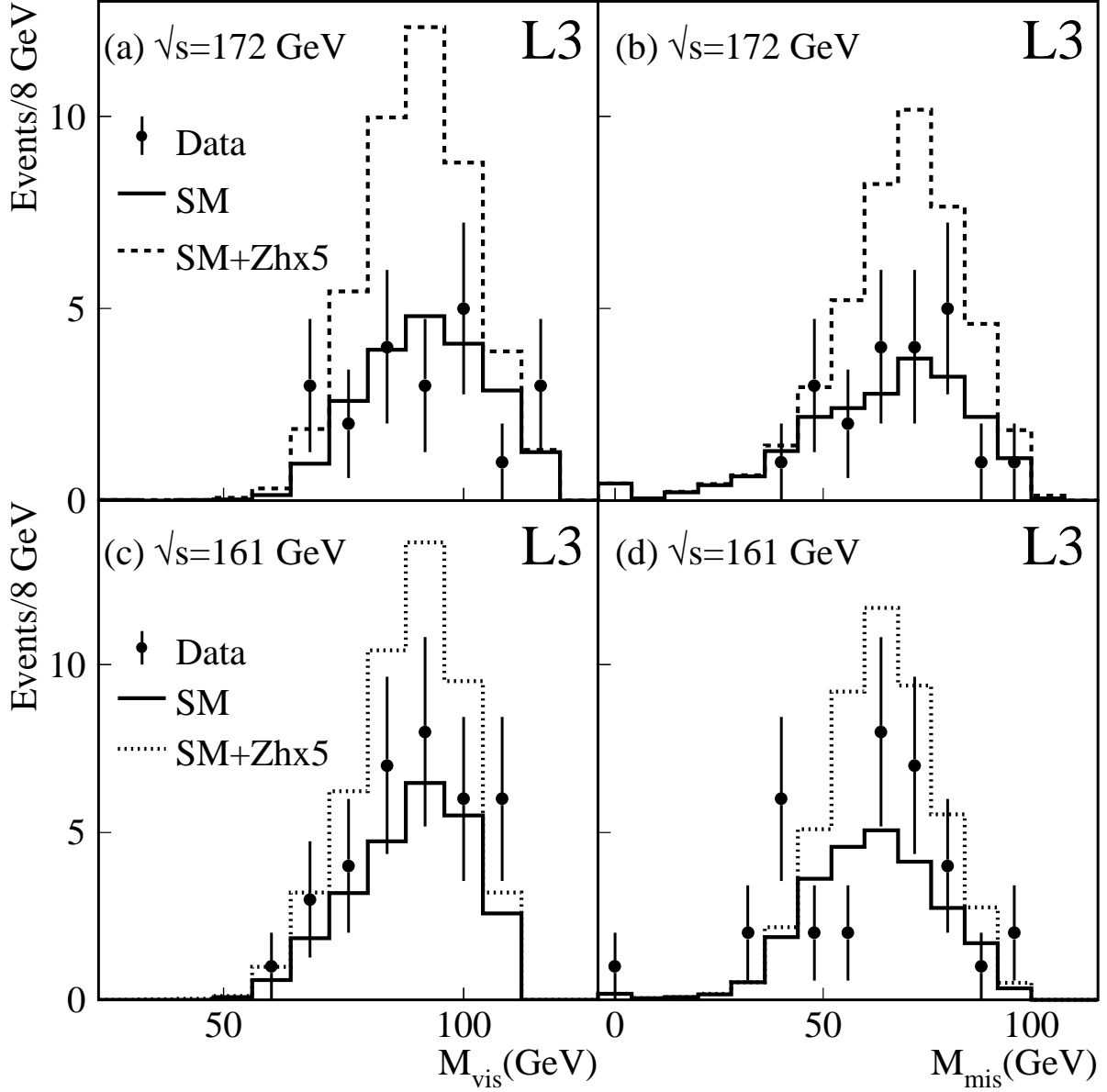


Figure 3: Distributions of the visible mass, (a), (c), and the missing mass, (b), (d), after selection cuts 1 through 6 (see text) at $\sqrt{s} = 172$ GeV and 161 GeV for the data (dots) compared to the sum of the Standard Model contributions (solid histogram) from fermion-pair and four-fermion productions. The sum of the Standard Model (SM) and the Higgs signal (Zh) contributions for a 70 (65) GeV Higgs signal, at $\sqrt{s} = 172$ (161) GeV, is shown by the dashed (dotted) histogram. The Higgs contribution is normalised to 5 times the actual luminosities using the Standard Model Higgs production cross section.

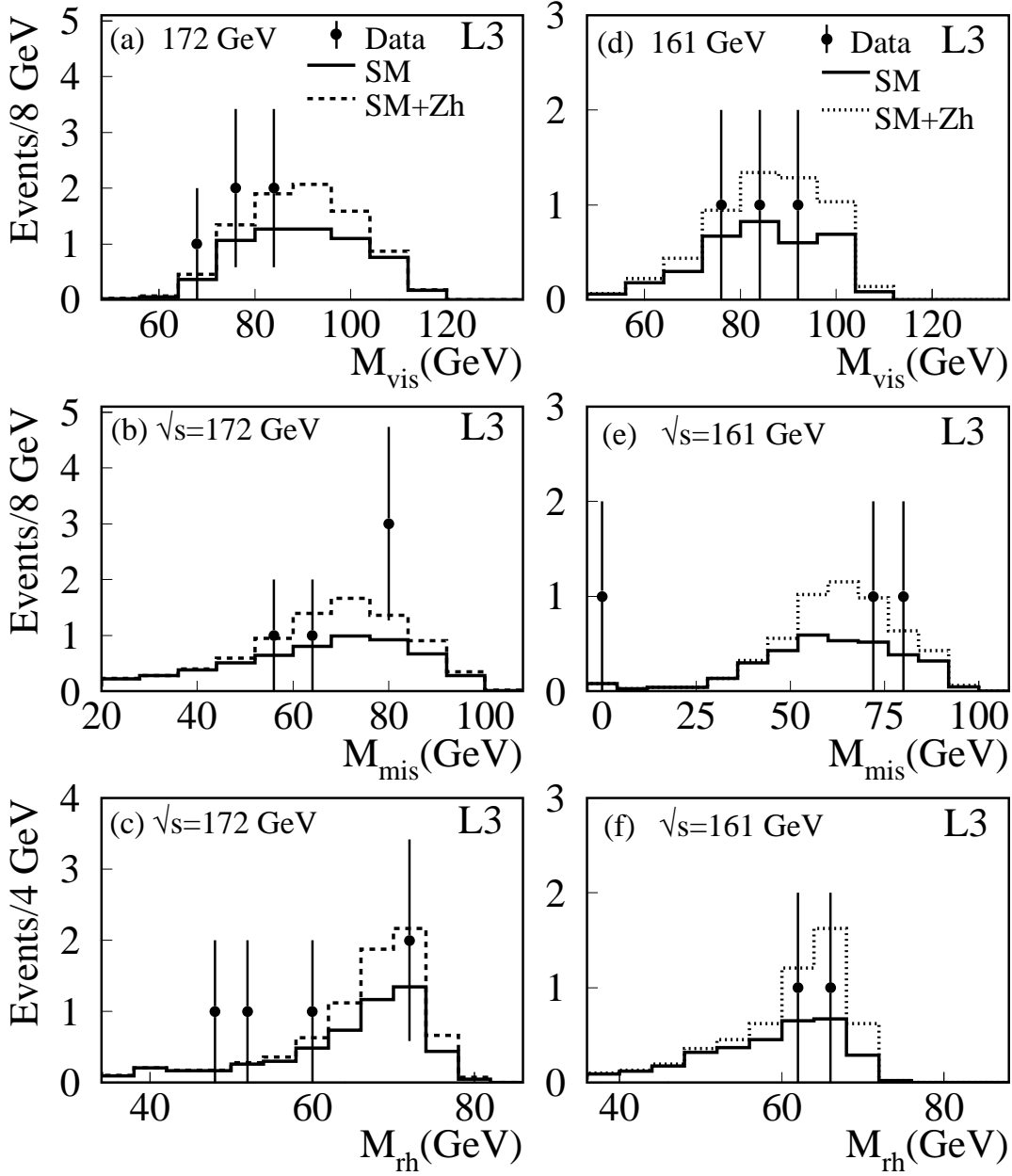


Figure 4: Distributions of the visible mass M_{vis} , (a) and (d), the missing mass M_{mis} , (b) and (e), and the reconstructed Higgs mass M_{rh} , (c) and (f), at $\sqrt{s} = 172$ GeV and 161 GeV. The data (dots) are compared to the sum of the Standard Model contributions (solid histogram). The sum of the Standard Model and the Higgs signal contributions, for a 70 (65) GeV Higgs at $\sqrt{s} = 172$ (161) GeV, is shown by the dashed (dotted) histogram. The Higgs contribution is normalised to the actual luminosities using the Standard Model Higgs production cross section.

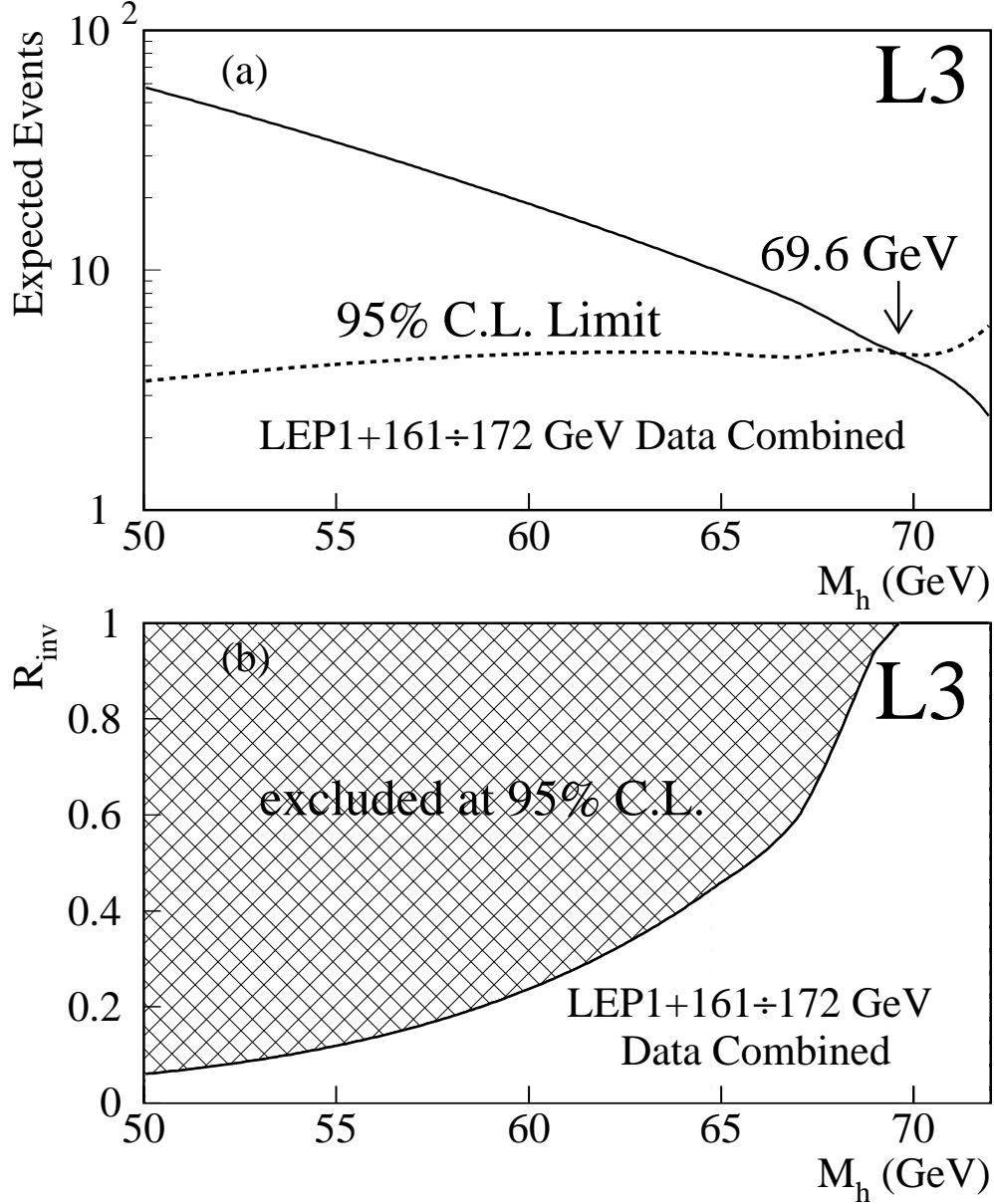


Figure 5: (a) The number of expected Higgs signal events (solid line), assuming Standard Model Higgs production cross section, and 100% decay branching fraction into invisible particles, and the 95% confidence level upper limit on the number of signal events (dashed line) as a function of the Higgs mass. This limit is set combining the 161-172 GeV with the LEP1 results of the search for invisible Higgs decays. (b) Upper limit on R_{inv} , the rate of invisible Higgs decays, relative to the Standard Model Higgs production rate.